Ⅲ-3

Chemistry

BL1U

Molecular Orientation Induced by Irradiation Polarized or Optical Vortex Wavelength Selective UV Light to Azo-metal Complexes in Polymer Films

T. Akitsu[1], S. Yagi[1], S. Yamazaki[1], M. Yoshida[1], T. Haraguchi[1], M. Fujiki[2], M. Fujimoto[3] and M. Katoh[3]

[1]*Faculty of Sciences, Tokyo University of Science, Tokyo 162-8601, Japan*
[2]*Graduate School of Materials Sciences, NAIST, Nara 630-0192, Japan*
[3]*UVSOR Synchrotron Facility, Institute for Molecular Science, Okazaki 444-8585, Japan*

In recent years, studies on photochemical materials using optical vortex UV light have attracted attention. In contrast to circularly polarized light, a light vortex having a spiral wave front and carrying an orbital angular momentum gives a torque when irradiated on photofunctional materials. In this context, we have attempted molecular orientation control by irradiating linearly and/or circularly polarized (and optical vortex) UV light to polymer films containing (chiral or achiral) dinuclear Schiff base metal complexes [1, 2] with/without azo-dyes exhibiting cis-trans photoisomerization and Weigert effect. Herein, we employed azo-containing mononuclear Schiff base metal complexes (Fig. 1) in PMMA films for molecular orientation phenomenon induced by several types of UV light irradiation.

We prepared them in the common procedures and measured their UV-vis spectra or other data. Among these four complexes, we selected a complex with M=Zn(II) and R=H (**PazZn**) appearing intense peak at 380 nm for the following photo-irradiation experiments. We have also checked cis-trans photisomerization of azo-moiety of ligand by wavelength selective UV light irradiation and Weigert effect, which is linearly polarized light induced anisotropic molecular orientation, and supramolecular chiral arrangement induced by circularly polarized light irradiation.

Based on these experiments using a conventional laboratory light source, the irradiation wavelength of the optical vortex was set to 317 nm, Δλ = about 30 nm. Photo-illumination with linearly polarized light (LPL), circularly polarized light (CPL), OV and optical vortex (OV) of UV light was carried out using UVSOR beam line BL1U as listed in Table 1. For example, Fig. 2. depicts typical results of CD spectra.

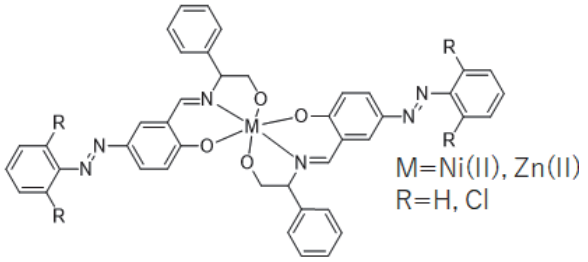

Fig. 1. Molecular structures of metal complexes.

Table 1. Experimental conditions.

	Sample	Light	Time/min	Condensing
1	PazZn	CPL	1	
2	PazZn	CPL	10, 10	
3	PazZn	CPL	10, 65	
4	PazZn	LPL	30	
5	PazZn	CPL	60	
6	PazZn	CPL	60	V
7	PazZn	CPL	60	V
8	PazZn	LPL	180	V
9	PMMA	CPL	60	
10	PazZn	OV	218	
11	PazZn	OV	201, 205	
12	PazZn	OV	267, 195	
13	PazZn	CPL	30, 30	V

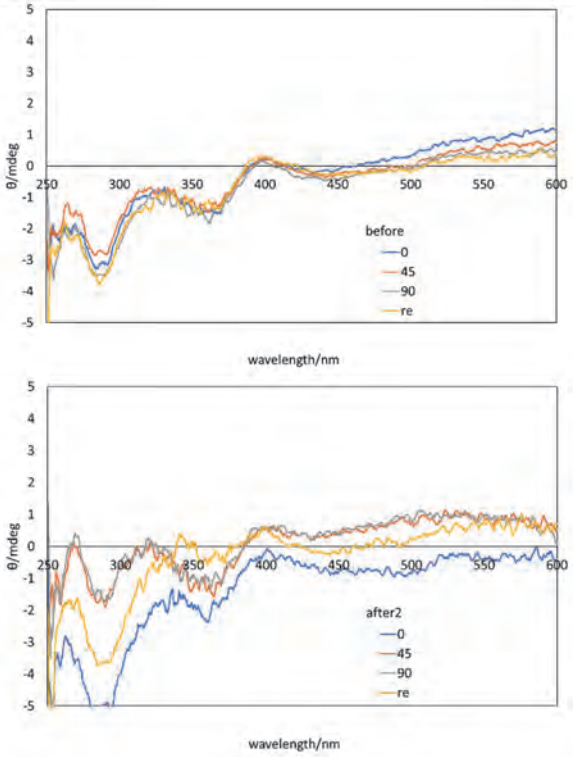

Fig. 2. CD spectra of **PazZn** under the condition 11 after 0 (above) and 205 (below) min.

[1] H. Nakatori, T. Haraguchi and T. Akitsu, Symmetry **10** (2018) 147.
[2] M. Takase, S. Yagi, T. Haraguchi, S. Noor and T. Akitsu, Symmetry **10** (2018) 760.

BL1U

Absolute Asymmetric Synthesis with Circularly Polarized Light

J. Yao and C. Yang

Key Laboratory of Green Chemistry & Technology of Ministry of Education, State Key Laboratory of Biotherapy, Sichuan University, Chengdu 610065, China

Circularly polarized light (CPL) is without doubt truly chiral electromagnetic radiation in the sense described above and therefore CPL should in theory be able to induce absolute asymmetric synthesis.[1] We have studied the chiral induction effects of circularly polarized light (CPL) for photo-responsive compounds (Fig. 1). The racemic compounds will be exposure in the CPL and to produce the excess enantiomer by the differential absorption and the process can be detected by CD spectra. We have irradiated 8 samples on these days and the presentationis as follows (Table 1).

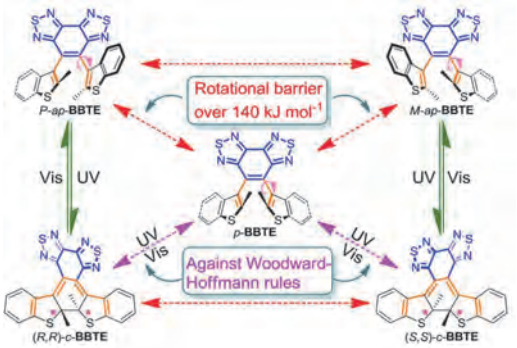

Fig. 1. Photo-Responsive Compounds.

Table 1. The Results of CPL Experiments.

Samples	Irradiations	CD spectra
1 (**YJB-4-41**)	R-CPL 1.6 mW 309 nm 5 min	No signal, Hexane
	R-CPL 1.6 mW 309 nm 35 min	No signal, Hexane (precipitate)
	R-CPL 3.6 mW 359 nm 30 min	No signal, Hexane
	L-CPL 3.6 mW 359 nm 3 min	No signal, Hexane
	L-CPL 3.5 mW 359 nm 10 min	No signal, Hexane
	L-CPL 2.4 mW 359 nm 30 s	No signal, Hexane
	L-CPL 3.5 mW 359 nm 3 min + L-CPL 0.58 mW 510 nm 2 min	No signal, Hexane
2 (**YJB-4-42**)	R-CPL 1.6 mW 309 nm 5 min	No signal, Hexane
	R-CPL 3.6 mW 359 nm 20 min	No signal, Hexane
	L-CPL 3.0 mW 359 nm 2 min	No signal, Hexane
	R-CPL 320 nm 3 min	No signal, Hexane
	R-CPL 359 nm 5 min	No signal, Hexane
3 (**YJB-4-39D**)	R-CPL 1.6 mW 309 nm 5 min	No signal, Hexane
4 (**HTT-5B**)	R-CPL 2.5 mW 309 nm 5 min	No signal, $CHCl_3$
	R-CPL 1.5 mW 280 nm 5 min	No signal, $CHCl_3$
5 (**HTT-7B**)	R-CPL 2.5 mW 309 nm 5 min	No signal, $CHCl_3$
6 (*ap*-**BBET**)	R-CPL 1.3 mW 280 nm 10 min	No signal, MeCN (color change)
	L-CPL 1.8 mW 280 nm 5 min + L-CPL 0.58 mW 510 nm 7+16 min	No signal, MeCN (color change)
	R-CPL 280 nm 5 min	No signal, MeCN (color change)
7 (Photoreaction)	R-CPL 280 nm 2.5 h + 5.5 h	Unconverted reactants
8 (Photoreaction)	L-CPL 280 nm 3.5 h + 4.5 h	Unconverted reactants

[1] M. Shapiro and P. Brunner, J. Chem. Phys. **95** (1991) 8658.

BL3U

Phase Transitions of Liquid-crystal Materials Studied by X-ray Absorption Spectroscopy

H. Iwayama[1,2], H. Yuzawa[1] and M. Nagasaka[1,2]

[1]*UVSOR Synchrotron Facility, Institute for Molecular Science, Okazaki 444-8585, Japan*

[2]*School of Physical Sciences, The Graduate University for Advanced Studies (SOKENDAI), Okazaki 444-8585, Japan*

In addition to gas, liquid and solid phases, liquid-crystal materials have liquid-crystal phase between solid and liquid phases. In the case of nematic liquid-crystals materials, the rod-shaped organic molecules have no position order, but they self-align to have long-range directional order with their long axes roughly parallel. During a phase transition, certain properties of materials change, often discontinuously, as a result of changes of a local chemical environment. Since X-ray absorption fine structure (XAFS) spectroscopy is sensitive to a local atomic geometry and the chemical state of the atom of one specific element, XAFS spectroscopy is suitable to investigate changes of structures of materials. In this work, we observe discontinuous changes of XAFS spectra for liquid-crystal materials.

Our sample is 4-Cyano-4'-pentylbiphenyl (5cb), which is one of the most popular liquid-crystal materials. A schematic draw of 5cb molecules is shown in Fig. 1. The phase transition temperature of liquid to liquid-crystal and liquid-crystal to solid are 22.5 and 35 °C, respectively. The XAFS measurements were carried out at BL3U [1]. After liquid cell which is composed of two Si3N4 membranes was filled with the liquid sample, the thickness of liquid sample was optimized by controlling the He gas pressure around the cell. The photon energy was calibrated by using the C-K edge XAFS spectrum of the proline thin layer.

Figure 2 shows C K-edge XAFS spectra of 5cb sample at three different temperature, which correspond to liquid, liquid-crystal and solid phases. We observed a strong peak at 285 eV, which correspond to a core excitation of C 1s to π* orbitals of phenyl group. It seems that the peak at 285 eV has two components, suggesting that π* orbitals of two benzene rings are different from the viewpoint of binding energies. As shown in Fig.2 intensities of the peak B clearly depend on sample's phases. To evaluate relative intensities of peak B, we performed fitting procedure with using two Gaussian functions.

Figure 3 shows a temperature dependence of peak intensities. We found discontinuous change around 22 °C. This temperature corresponds to the phase transition temperature between solid and liquid-crystal phases. During a phase transition between solid and liquid-crystal, sample lose position order. As a results, local chemical environment change discontinuously. A more detail analysis is now in progress.

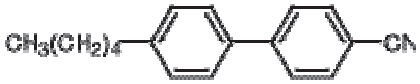

Fig. 1. Schematic draw of 4=Cyano-4'- pentylbiphenl (5cb) molecules.

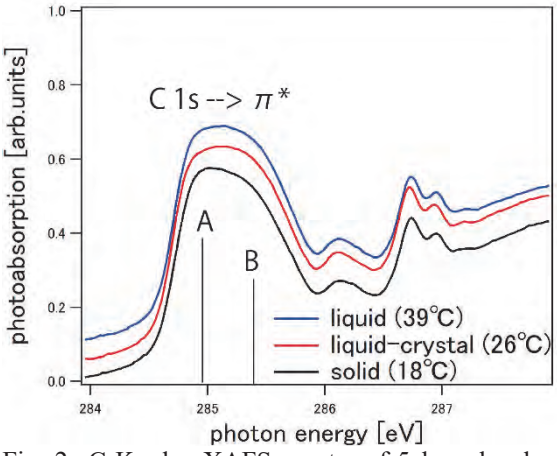

Fig. 2. C K-edge XAFS spectra of 5cb molecules at 18 (solid), 26 (liquid-crystal) and 39 °C (liquid).

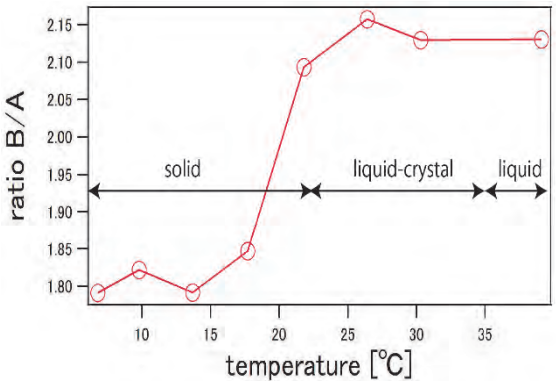

Fig. 3. Temperature dependence of peak B.

[1] M. Nagasaka, H. Yuzawa and N. Kosugi, J. Spectrosc. Relat. Phenom. **200** (2015) 293.

BL3U

Local Structures of Aqueous Acetonitrile Solutions Probed by Soft X-ray Absorption Spectroscopy

M. Nagasaka[1,2], H. Yuzawa[1] and N. Kosugi[1,2]
[1]*Institute for Molecular Science, Myodaiji, Okazaki 444-8585, Japan*
[2]*The Graduate University for Advanced Studies (SOKENDAI), Myodaiji, Okazaki 444-8585, Japan*

Aqueous acetonitrile solution is one of the most basic systems showing the microheterogeneity (MH) state, where two liquids are mixed at macroscopic scale but are not mixed in microscopic scale [1]. It is necessary to observe molecular interactions between acetonitrile and water to discuss the mechanism of the MH state. The previous studies of infrared spectroscopy and X-ray diffraction [2] indicate that acetonitrile molecules form two structures with water: One is hydrogen bond (HB) between N atom of acetonitrile with H atom of water. The other is the dipole (DP) interaction between C≡N group of acetonitrile with water. Recently, Huang *et al.* proposed that the population of DP structure is larger than that of HB structure from O K-edge X-ray absorption spectroscopy (XAS) [3]. However, O K-edge XAS only gives the molecular interactions from the water side. In this study, we have measured XAS of aqueous acetonitrile solutions at both C and N K-edges in order to discuss molecular interactions from acetonitrile side.

The experiments were performed at soft X-ray beamline BL3U. XAS of liquid samples were measured by a transmission-type liquid flow cell [4]. The liquid layers were sandwiched between two 100 nm-thick Si_3N_4 and SiC membranes for XAS at C and N K-edges, respectively. In order to keep the same X-ray absorbance even at different concentrations, the thickness of the liquid layer was controlled by adjusting the He pressure around the liquid cell.

Figure 1 shows the energy shifts of the C≡N π* peaks of aqueous acetonitrile solutions at different concentrations $(CH_3CN)_x(H_2O)_{1-x}$ from the neat liquid (x = 1.0). In the C K-edge XAS, three concentration regions are found with the borders of $x = 0.7$ and $x = 0.2$. In the acetonitrile-rich region I ($1.0 > x > 0.75$), the π* peaks in C K-edge shows slightly lower energy shifts by increasing molar fraction of water, and suddenly shows a higher energy shift at $x = 0.7$. On the other hand, the π* peaks in N K-edge show higher energy shifts and show no phase transition-like behavior at $x = 0.7$. In the region II ($0.7 > x > 0.25$), the energy shifts of the π* peaks in both C and N K-edges are gently increased. Note that this concentration region shows the MH behavior [1]. In the water-rich region III ($0.2 > x > 0.05$), the slope of the energy shifts in C K-edge is rapidly increased whereas that in N K-edge is not changed.

We have performed inner-shell calculations of acetonitrile-water mixtures to discuss local structures of acetonitrile at different concentrations in terms of the energy shift in C and N K-edges. As a result, isolated water molecules disturb the interaction between acetonitrile molecules in the region I. The acetonitrile clusters are surrounded by water molecules with the DP interactions between acetonitrile and water in the region II. Small acetonitrile clusters form the HB interactions with water in the HB network of water in the region III. Since the DP interaction is abundant in the region II, the DP interaction is a key factor to form the MH state in aqueous solutions.

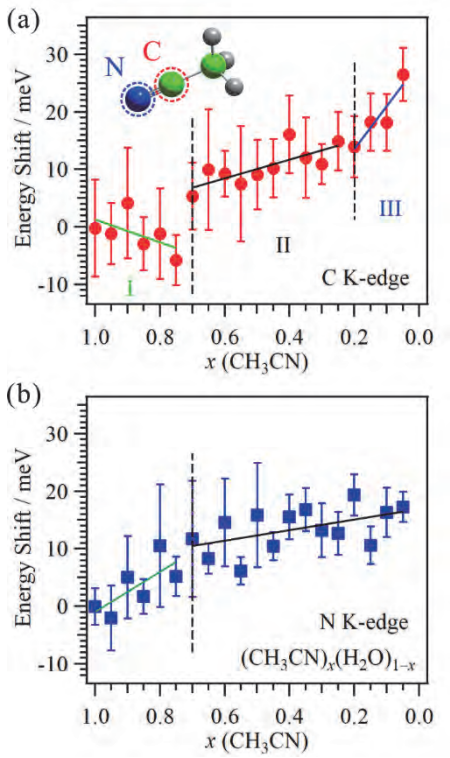

Fig. 1. Energy shifts of the peaks in XAS of aqueous acetonitrile solutions $(CH_3CN)_x(H_2O)_{1-x}$ relative to the peak of neat liquid (x = 1.0) at (a) C and (b) N K-edges. Three concentration regions are found with the borders of $x = 0.7$ and $x = 0.2$.

[1] Y. Marcus, J. Phys. Org. Chem. **25** (2012) 1072.
[2] T. Takamuku *et al.*, J. Phys. Chem. B **102** (1998) 8880.
[3] N. Huang *et al.*, J. Chem. Phys. **135** (2011) 164509.
[4] M. Nagasaka *et al.*, J. Electron Spectrosc. Relat. Phenom. **224** (2018) 93.

BL3U

Effect of Salt Addition on the Electronic Structure of the Hydrated Water of Glycine Betaine Studied by Soft X-Ray Absorption Spectroscopy

S. Ohsawa[1], N. Fukuda[1], H. Iwayama[2,3], H. Yuzawa[2], M. Nagasaka[2,3] and K. Okada[1]
[1]*Graduate School of Science, Hiroshima University, Higashi-Hiroshima 739-8526, Japan*
[2]*Institute for Molecular Science, Okazaki 444-8585, Japan*
[3]*School of Physical Sciences, The Graduate University for Advanced Studies (SOKENDAI), Okazaki 444-8585, Japan*

Most living cells adapt to various environments, such as drought and high salinity, by regulating the concentration of solutes termed osmolytes [1], because an increase in extracellular salinity can cause water efflux and cell shrinkage. Among the most common organic osmolytes is glycine betaine, which is a zwitterionic quaternary ammonium species with pK_a = 1.84. Its accumulation occurs either by synthesis from choline or by transport from extracellular pools [2]. The amount of glycine betaine has been found to correlate with external salinity for several shoots of halophytes [3] and for halophilic eubacteria [4]. Altering the hydration structure of glycine betaine with the salt concentration presumably plays an important role in protecting the secondary structure of proteins, but the details of interactions of the osmolyte with surrounding water along with salt ions are not yet fully understood.

Photoabsorption spectra at the oxygen K-edge were measured in the transmission mode at room temperature. Aqueous solutions of glycine betaine, sodium chloride, and mixed glycine betaine and sodium chloride were introduced with a tubing pump system into a liquid flow cell installed on the soft X-ray beamline BL3U. The flow cell for this study was equipped with a pair of windows made of thin silicon nitride membrane. Further details of the cell were given elsewhere [5]. The incident photon energy was calibrated to the peak at 530.88 eV of a polymer film [6].

The measured absorption spectra vary from solution to solution. Figure 1 displays the O 1s absorption spectra of glycine betaine, sodium chloride, their mixed aqueous solutions, and liquid water. The broken vertical line corresponds to the resonance energy of the $4a_1 \leftarrow$ O 1s transition of bulk water located at 534.6 eV. For solutions containing glycine betaine, another broad peak appears around 532.2 eV. Because its intensity depends on the osmolyte concentration, the peak is safely assigned to $\pi^*_{COO} \leftarrow$ O 1s of glycine betaine.

The resonance peak top of water is shifted by −0.05 and +0.09 eV for glycine betaine and sodium chloride solutions, respectively. The shift is caused by the change of chemical environment around water. The red shift seen for the glycine betaine solution can be ascribed to the gain of partial negative charge on the oxygen atom of water by making a strong hydrogen bond with the carboxylate site of glycine betaine.

For the mixed aqueous solutions, an apparent blue shift can be seen for the spectra of samples with the salt concentration greater than or equal to the osmolyte concentration. This observation can be described by the interpretation that the salt is exclusively bound to glycine betaine, and thereby reveals the role of the osmolyte when living cells are exposed to salinity.

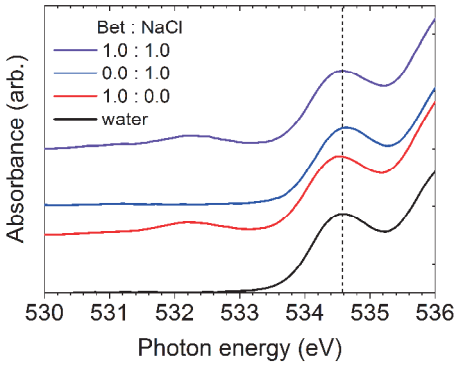

Fig. 1. Enlarged O 1s photoabsorption spectra in the 530–536 eV region of glycine betaine (Bet), sodium chloride, their mixed aqueous solutions, and liquid water. The concentration of each solute is 1.0 mol/L.

[1] P. H. Yancey, M. E. Clark, S. C. Hand, R. D. Bowlus and G. N. Somero, Science **217** (1982) 1214.
[2] L. N. Csonka, Microbiol. Rev. **53** (1989) 121.
[3] R. Storey and R. G. Wyn Jones, Plant Sci. Lett. **4** (1975) 161.
[4] J. F. Imhoff and F. Rodriguez-Valera, J. Bacteriol. **160** (1984) 478.
[5] M. Nagasaka, T. Hatsui, T. Horigome, Y. Hamamura and N. Kosugi, J. Elec. Spectrosc. Relat. Phenom. **177** (2010) 130.
[6] M. Nagasaka, H. Yuzawa, T. Horigome and N. Kosugi, J. Elec. Spectrosc. Relat. Phenom. **224** (2018) 93.

BL3U

X-ray Absorption Measurements Applied to Aqueous Solutions of Glycine at Various pHs, in the Vicinity of the O K-edge Ionization Thresholds

D. Céolin[1], T. Saisopa[2], K. Klaiphet[2], P. Songsiriritthigul[2], H. Yuzawa[3], M. Nagasaka[4] and N. Kosugi[4,5]

[1]*Synchrotron SOLEIL, L'Orme des Merisiers Saint-Aubin BP 48 91192 Gif-sur-Yvette Cedex, France*
[2]*Research Network NANOTECH-SUT on Advanced Nanomaterials and Characterization and School of Physics, Suranaree University of Technology, Nakhon Ratchasima 30000, Thailand*
[3]*UVSOR Synchrotron Facility, Institute for Molecular Science, Okazaki 444-8585, Japan*
[4]*Institute for Molecular Science, Okazaki 444-8585, Japan*
[5]*Institute of Materials Structure Science, KEK, Tsukuba 305-0801, Japan*

Glycine, the simplest amino acid, is involved in a variety of physiological processes, such as e.g. neurotransmitter in the central nervous system, and is commonly found as a protein precursor. Gas-phase glycine has a neutral form H_2N-CH_2-COOH whereas in aqueous solution its structure differs depending on the pH. For pH in the range 2.4-9.6, the zwitterionic form ^+H_3N-CH_2-COO^- dominates. In acidic medium below pH = 2.4, the protonated form ^+H_3N-CH_2-COOH is the main one, whereas in basic medium above pH = 9.6, the deprotonated form H_2N-CH_2-COO^- prevails (see Fig. 1).

Among our measurements performed at the beamline BL3U using the liquid cell in transmission mode, we obtained the absorption spectra of glycine in aqueous solution at different pH, at a concentration of 0.5 M, and in the vicinity of the O *K*-edge ionization threshold (see Fig. 2). The idea was to collect spectra in a larger energy window than in the reference [1].

The resonance located at hν = 535 eV is associated with the oxygen 1s electron excitation of water to its first empty orbital. On the left side of this structure, we confirm the presence of smaller resonances attributed to the excitation of an oxygen 1s electron of the carboxyl/carboxylate groups of solvated glycine. The O1s→π* excitation of $–COO^-$ leads to a maximum located at 532.75 eV, whereas for –COOH the maximum is found at 532.45 eV. For this latter, only the transition involving the C=O group is visible. The one corresponding to the –OH excitation is located at a photon energy close to the one of water and is thus not detected in our spectra.

Contrary to the observations presented in reference [1], due to a reduced statistic, we do not highlight a clear asymmetry of the low energy resonance in the acidic solution. However, we can extract some additional information such as the $–COO^-$/–COOH O1s→π* widths (Gaussian FWHM): 0.85 eV for pH = 1, 1.21 eV for pH = 7 and 1.25 eV for pH = 12, and the corresponding relative areas: 0.52 for pH = 1, normalized to 1 for pH = 7, and 0.77 for pH = 12. Considering that the –OH part of the carboxylic group do not resonate in this photon energy region, the lower intensity of the 1st structure for the acidic solution is not surprising. Furthermore, the larger contribution of the same resonances for the two other solutions is due to the possibility of exciting two oxygens instead of only one. Also, the overlap with the 2nd large resonance having a maximum at 535 eV increases the uncertainty of the areas estimate especially for the solutions at pH = 7 and 12 since they are located closer in photon energy.

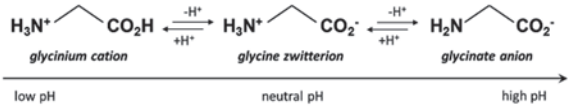

Fig. 1. Structure of glycine in aqueous solution for various pH regions (acidic, neutral, basic).

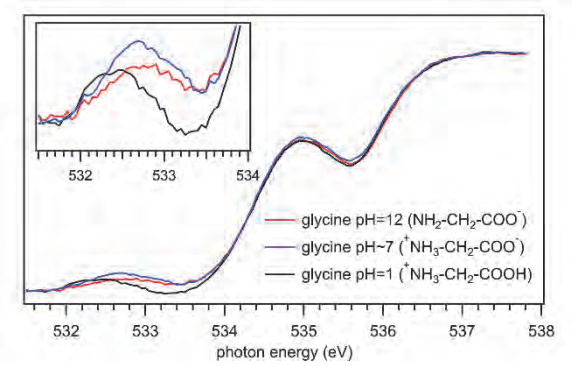

Fig. 2. Normalized X-ray absorption spectra of solvated glycine, recorded for various solutions pH.

[1] B. M. Messer, C. D. Cappa, J. D. Smith, K. R. Wilson, M. K. Gilles, R. C. Cohen and R. J. Saykally, J. Phys. Chem. B **109** (2005) 5375.
[2] M. L. Gordon, G. Cooper, C. Morin, T. Araki, C. C. Turci, K. Kaznatcheev and A. P. Hitchcock, J. Phys. Chem. A **107** (2003) 6144.

BL3U

In situ O K-edge X-ray Absorption Spectrum Study of a-Si/SEI in Photocatalytic Water Splitting

J. Ma[1], H. Yuzawa[2], H. Ju[1] and R. Long[1]

[1] *Hefei National Laboratory for Physical Sciences at the Microscale, iChEM (Collaborative Innovation Center of Chemistry for Energy Materials), School of Chemistry and Materials Science, and National Synchrotron Radiation Laboratory, University of Science and Technology of China, Hefei, Anhui 230026, China*

[2] *UVSOR Synchrotron Facility, Institute for Molecular Science, Okazaki 444-8585, Japan*

Amorphous Si/SEI (a-Si/SEI) nanowire arrays was fabricated and both activity and durability of silicon material for photocatalytic water splitting can be dramatically enhanced. The Si nanoarrays were first loaded in a battery cell, then facilely engineered into active and durable structures, during which lithiation amorphizes silicon and forms a surface protection layer. The photocatalytic hydrogen production was conducted to assess the performance of the as fabricated Si NWs for photocatalytic hydrogen production in ultrapure water. Remarkably, the processed silicon nanowire arrays achieve an apparent quantum efficiency (AQE) of 1.74% in pure water under 450 nm light irradiation with excellent durability. The lithiated Si NWs achieved a hydrogen production rate of 6.0 μmol·h^{-1} at the first reaction cycle. However, hydrogen production rate was reduced to 3.4 μmol·h^{-1} in the second reaction cycle and became stable thereafter as indicated by the next 50 h of test.

Then the X-ray photoelectron spectroscopy (XPS) was conducted to characterize surface of the discharged Si NWs which plays a significant role in the photocatalytic hydrogen production. As revealed in Fig. 1, the Si NWs samples before reaction (a), after reaction 4 h (b) and 20 h (c) radiation were measured by in-house XPS.

We can observe the Si at 99 eV binding energy assigned to bulk amorphous silicon, the peak at 103 eV binding energy assigned to surface oxide SiO2, the peak at ~101.5 eV binding energy assigned to the lithium orthosilicate Li_4SiO_4 and the peak at ~105 eV binding energy assigned to the partially fluorinated compound SiO_xF_y located at the extreme surface. The relative intensity of the partially fluorinated compound SiO_xF_y became weaker. And the relative intensity of other Si species changes dramatically after photocatalytic reaction. Indeed the bulk amorphous silicon species relative intensity has significant increase after photocatalytic reaction and stay almost unchanged as the photocatalytic reaction goes on which can be attributed to the change of LiF in solid electrolyte interphase (SEI) during the photocatalytic reaction, and the partially fluorinated compound SiO_xF_y species relative intensity obviously weakens at the begin of the reaction and then keeps constant while the relative intensity of the surface oxide SiO_2 and the lithium orthosilicate Li_4SiO_4 appears no obvious change during the reaction.

To further observe the evolution of the surface condition during the photocatalytic reaction, the in situ near edge X-ray absorption fine structure (NEXAFS) was conducted at UVSOR Synchrotron Facility. As shown in Fig. 2, the in situ O K-edge XAS was collected before and after illumination in the chamber. We can see that peaks of SiO_2, Li_4SiO_4 and SiO_xF_y from the spectra. However, the peaks of SiO_xF_y obviously became weaker assigned to reduction of content, which can is consistent with the X-ray photoelectron spectroscopy. And the peak of Li_4SiO_4 almost disappeared after illumination owing to the meager content Li_4SiO_4 and weak signal. Overall, the intensity of SiO_xF_y decreases significantly at the reaction starting indicating reduction of SiO_xF_y which we think can well explain the drop of photocatalytic hydrogen production rate at first cycle. The other species remain basically unchanged and these species can reasonably protect the innermost amorphous from photocorrosion.

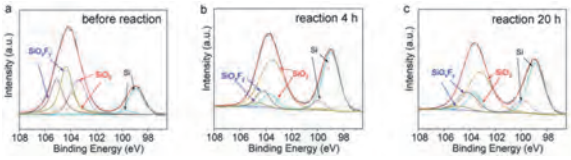

Fig. 1. XPS spectra evolution during reaction.

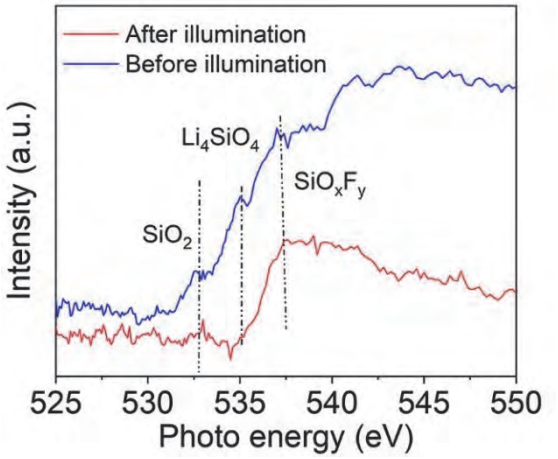

Fig. 2. In situ O K-edge X-ray absorption spectra.

BL3U

Mechanistic Investigation of Homogeneous Iron-Catalyzed Organic Reactions based on Solution-Phase L-edge XAS

H. Takaya[1], M. Nagasaka[2] and K. Kashimura[3]

[1]*International Research Center for Elements Science, Institute for Chemical Research, Kyoto University, Uji 611-0011, Japan*

[2]*UVSOR Synchrotron Facility, Institute for Molecular Science, Okazaki 444-8585, Japan*

[3]*Faculty of Engineering, Chubu University, Kasugai 487-8501, Japan*

We have found that iron complexes of FeX_2SciOPP (X = Cl, Br) bearing bulky phosphine ligand SciOPP showed excellent catalytic activities toward the cross-coupling of organometallic reagents of Mg, B, Al, and Zn with various aryl halides (Eq. 1) [1, 2]. Such iron-based catalysts for organic reactions alternative to the conventional precious metal catalysts has been intensively investigated for the development of future sustainable chemical processes. Solution-phase XAS analysis is highly useful for the mechanistic study of iron-catalyzed organic reactions to identify the catalytically active organoiron species with their electronic and molecular structures, because the conventional solution-phase NMR-based analysis cannot be used due to the paramagnetic nature of organoiron species along with the large paramagnetic shift and peak broadening in NMR spectrum. L-edge XAS of transition-metal catalysts has been expected to be highly useful to investigate the electronic structure of 3d orbitals which provide an essential information to elucidate how to work the catalyst. However, solution-phase L-edge XAS measurement is generally difficult because the measurement has to be performed under low-pressure vacuum condition where the solution sample is evaporated with vigorous boiling. In this project, we used the specially designed flow-cell for the solution-phase L-edge XAS measurement of homogeneous organic solution of iron complex catalysts. In BL3U beamline, a stainless-steel flow cell has been used for various experiments, but we should carefully avoid contamination of iron species from the environment. For this reason Prof. Nagasaka newly designed and prepared PEEK-made flow cell bearing ultra-thin 100 nm Si_3N_4 membrane X-ray window as shown in Fig. 1. The solvent-resistant PEEK made body shows an excellent chemical resistance toward the various organic solvents such as THF, CH_2Cl_2, and benzene, these often used in iron-catalyzed cross-coupling reactions. This flow cell was introduced into the helium-filled chamber which inserted to the X-ray optics line, and connected to syringe pump through a Teflon tube. The THF solution sample of $FeCl_2$SciOPP was prepared in an argon-filled glovebox, because this type of iron complex in solution is quite sensitive to oxygen and water, and immediately react to give iron oxide and hydroxide. The L-edge XAS experiment was carried out both stop and flow (flow rate: 50 – 500 μL/h) conditions to validate the XAS stabilities, base line moving, S/N change etc. As a result, a serious spectrum change and base line jump randomly occurred to interfere the stable XAS measurement by penetration of helium gas in chamber into the cell and made a bubble inside the sample space to cut across X-ray beam. To solve this problem, the Viton O-ring is changed to a fluorosilicone polymer with improving the flow line design and tube connection. This improved cell will be tested in the next experiment scheduled in 2019.

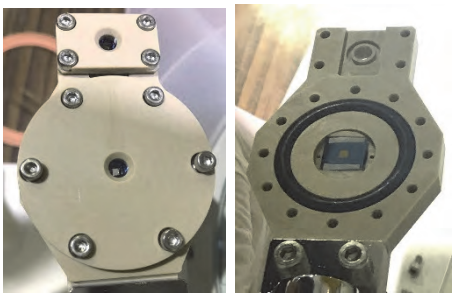

Fig. 1. Photo of the PEEK-made flow.

[1] H. Takaya and M. Nakamura *et al.*, Bull. Chem. Soc. Jpn. **88** (2015) 410.
[2] R. Takaya and M. Nakamura *et al.*, Bull. Chem. Soc. Jpn. **92** (2019) 381.

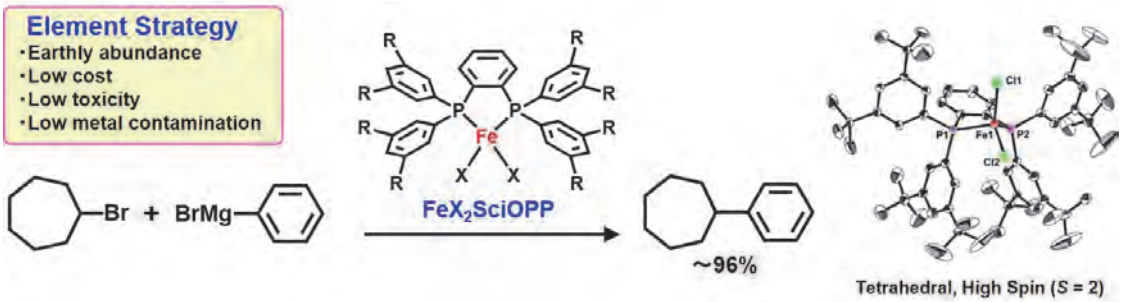

BL3U

Electronic Structures of Carbon Dots in Aqueous Dispersions Probed by *in-situ* Transmission X-ray Absorption Spectroscopy

J. Ren[1], D. S. Achilleos[2], E. Reisner[2] and T. Petit[1]

[1]*Institute of Methods for Material Development, Helmholtz-Zentrum Berlin für Materialien und Energie GmbH, Albert-Einstein-Strasse 15, 12489 Berlin, Germany*

[2]*Christian Doppler Laboratory for Sustainable SynGas Chemistry, Department of Chemistry, University of Cambridge, Lensfield Road, Cambridge CB2 1EW, UK*

Carbon dots (CDs) are promising photocatalysts for artificial photosynthesis since they are (1) inexpensive and non-toxic, (2) chemically and photochemically robust, (3) show good water solubility and (4) controlled photocatalytic properties upon pre-designed synthesis. Recently, we reported a facile method to prepare CDs of controlled nanostructures and elemental compositions by varying the organic precursors and the calcination temperatures employed for the synthesis. This approach allows the synthesis of graphitic CDs with (*g*-N-CDs) and without (*g*-CDs) core nitrogen doping, as well as amorphous CDs (*a*-CDs), which all show very distinctive photocatalytic properties.[1]

During this beamtime, colloidal dispersions of these three CDs were successfully characterized by soft X-ray absorption spectroscopy (XAS) at different concentrations. Both the carbon and oxygen K edges were characterized to monitor the impact of hydration on the electronic structure of both CDs and water molecules. Furthermore, these measurements were compared to XAS performed in total electron yield in vacuum and total ionic yield in liquid at BESSY II synchrotron, Germany.

XAS at the C K edge demonstrates that the core of the CDs is poorly influenced by the aqueous dispersion. On the other hand, electronic states associated with C-O bonds from surface groups appear enhanced in dispersion, which is attributed to the formation of hydrogen bonds with water molecules in their solvation shell.

At the O K edge, the signature of the CDs surface groups is screened by the contribution from water molecules (Fig. 1). However, strong changes on the water signature, composed of a pre-, main- and post-edges were found to depend on CDs as well as concentration. We previously observed similar changes in nanodiamonds colloidal dispersions and attributed them to strong changes of the water hydrogen bond network induced by the nanoparticles hydration.[2] These new results suggest that CDs also significantly interact with water molecules in their solvation shells.

These results are the first demonstration that carbon dots interact strongly with their hydration shell and the first *in situ* XAS characterization of CDs. Based on these results, an article has recently been submitted for publication.

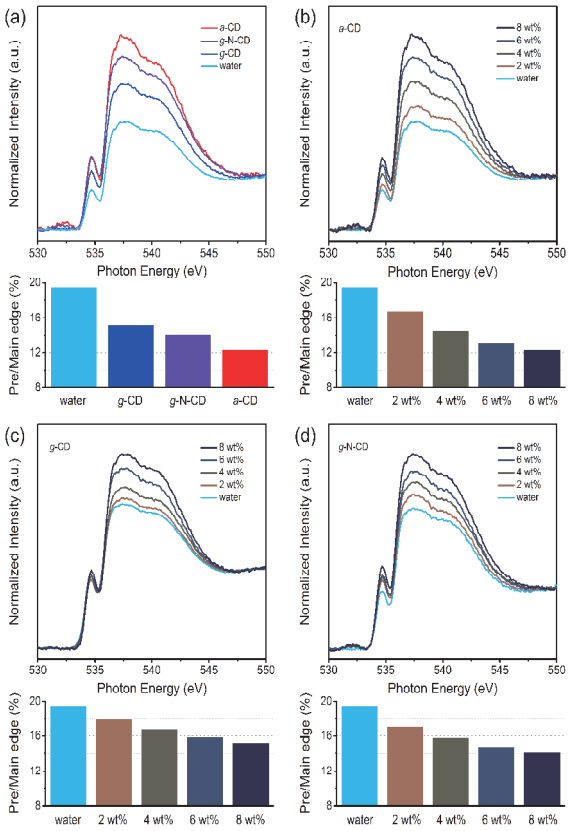

Fig. 1. Transmission mode XA spectra at O K-edge from (a) water and different CDs dispersions (8 wt%) and (b) *a*-CD, (c) *g*-CD, (d) *g*-N-CD at different concentrations. The pre/main-edge ratios for each spectrum are plotted below XA spectra.

[1] B. C. M. Martindale, G. A. M. Hutton, C. A. Caputo, S. Prantl, R. Godin, J. R. Durrant and E. Reisner, Angew. Chemie Int. Ed. **56** (2017) 6459.

[2] T. Petit, H. Yuzawa, M. Nagasaka, R. Yamanoi, E. Osawa, N. Kosugi and E. F. Aziz, J. Phys. Chem. Lett. **6** (2015) 2909.

BL4U

P-$L_{2,3}$ Absorption Spectra of Phosphates in Plasmid DNA and Cell Nucleus

T. Ejima[1], M. Kado[2], T. Ohigashi[3] and S. Tone[4]
[1]*IMRAM, Tohoku University, Sendai 980-8577, Japan*
[2]*Takasaki Adv. Rad. Res. Inst., QST, Takasaki 370-1292, Japan*
[3]*UVSOR Synchrotron Facility, Institute for Molecular Science, Okazaki 444-8585, Japan*
[4]*Sch. of Sci & Technol., Tokyo Denki University, Hatoyama 350-0394, Japan*

Phosphate PO_4^{3-} plays a major role in the structural framework of DNA and RNA. DNA in living cells is mainly present in cell nuclei, and phosphate PO_4^{3-} is contained in DNA, RNA, and some phosphorated proteins among the constituent molecules of cell nuclei [1]. On the other hand, DNA exists alone in bacteria and yeast, and this DNA, called plasmid DNA, is present in the cytoplasm and replicates itself autonomously and independently of genomic DNA [2].

The phosphate PO_4^{3-} forms ideally a tetrahedral structure in which four oxygen atoms coordinate equidistantly with a P atom as the center. The absorption spectrum excited at the P-$L_{2,3}$ absorption edge shows an electronic structure reflecting the s or d orbitals of the P atoms by the dipolar transition. Furthermore, if the chemical bonding states of a material is changed, the energy position of absorption edge will shift. In this study, the electronic structures and the chemical bonding states of the phosphate are compared by the P-$L_{2,3}$ absorption edge structures between the cell nucleus and the plasmid DNA.

As measurement samples, plasmid DNA extracted from *E. coli* and cell nuclei separated from Hela cells were dispersed in TE solutions, and the solutions of 0.5 μL each were dropped on 50 nm thick SiN membranes and then air-dried as it were. X-ray absorption measurements were performed using STXM beamline of BL4U under the experimental conditions: energy resolution E / δE = 1000, and spatial resolution 50 nm, and under He atmosphere. The obtained spectra are shown in Fig. 1.

The spectral intensity of plasmid DNA increases sharply at around 133 eV, and structures observed are indicated as Peak A ~ D in the figure. Peak intensity increases from Peak A to Peak D and decreases gradually on the higher energy side of Peak D (Fig. 1 (a)). The spectrum shape of the normal cell nucleus likes that of the plasmid DNA, but no explicit peak structures can be seen corresponding to Peak A~ D observed in the plasmid DNA (Fig. 1 (b)). A broad structure is observed (Peak E) with a broad shoulder structure (Peak F). In the plasmid DNA spectrum, spectral intensities of Peak E and F are weak, and the spectral shape looks as a part of the tail of Peak D.

The similar structures of the spectral shapes can be recognized by the tetrahedral coordination of the phosphate PO_4^{3-} in DNA [3]. The different structures will be due to the phosphate PO_4^{3-} of the protein molecules other than DNA in the cell nucleus.

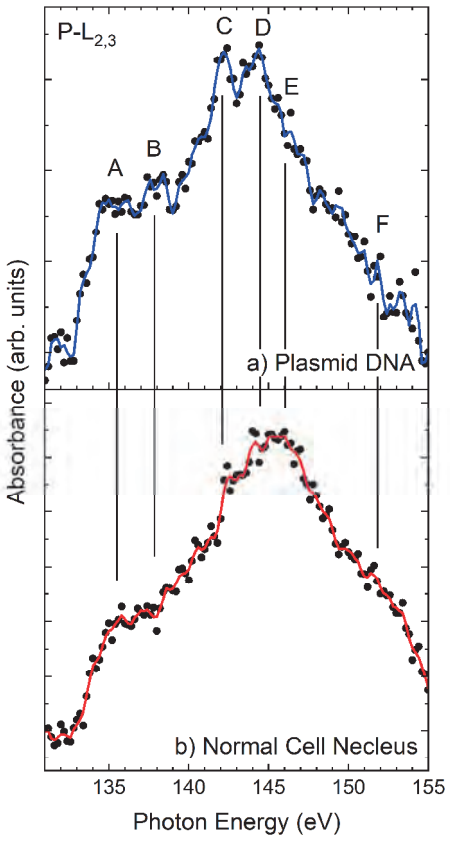

Fig. 1. P-$L_{2,3}$ X-ray absorption spectrum of plasmid DNA, (a), and of normal cell nucleus (b). Dots represent the measurement results, curves are 5 point smoothing results of the measurement points for guide to see. Both spectra are normalized by the maximum peak height around 145 eV.

[1] K. Shinohara, S. Toné, T. Ejima, T. Ohigashi and A. Ito, Cells **16** (2019) 164.
[2] for example, K. Akasaka and Y. Ohyama, "Principle of Gene Technology", (Syoukabo Co. Ltd., 2013, Tokyo, ISBN 978-4-7853-5856-3 C3045).
[3] S. O. Kucheyev, C. Bostedt, T. van Buuren, T. M. Willey, T. A. Land, L. J. Terminello, T. E. Felter, A. V. Hamza, S. G. Demos and A. J. Nelson, Phys. Rev. B **70** (2004) 245106.

BL4U

Heterogeneous Network Structure in Natural Rubber

Y. Higaki[1] and A. Takahara[2]

[1]*Department of Integrated Science and Technology, Faculty of Science and Technology, Oita University, Oita 870-1192, Japan*

[2]*Institute for Materials Chemistry and Engineering, Kyushu University, Fukuoka 819-0395, Japan*

Natural rubber (NR) latex is a liquid rubber product applied for thin rubber sheets and adhesives. The NR latex is a colloid of NR particles dispersed in serum including proteins, lipids, inorganic salts[1]. NR particles consist of a spherical core of poly(cis-1,4-isoprene) and outer shell membrane of a protein-lipid monolayer of approximately 20 nm thickness. The stable dispersion of NR particles is encouraged by the negatively charged substances covered on the surface. Because the NR sheets are produced by the coagulation of the NR particles involving protein and/or lipid shell, the NR sheets would exhibit heterogeneous network with boundary consisting of protein and lipids. In addition, the network structure through C-S, C-S-S bonds produced by vulcanization would be hardly uniform in the rubber matrix. We tried to address the heterogeneous chemical structure distribution in the NR sheets by cross-sectional chemical imaging of the NR sheets by means of scanning transmission X-ray microscopy (STXM) with soft X-ray.

NR particles, of which the averaged particle size is approximately 200 nm, were introduced into a glass dish then dried up subsequently vulcanized with sulfur to produce a vulcanized natural rubber sheet (thickness: 500 μm). The NR sheet was trimmed without embedding in resin by ultramicrotome to prepare ultra-thin film (setting thickness: 100 nm). The thin films were mounted on a copper grid without collodion supporting membrane (Ohken, Cu 100-A).

STXM experiments were performed at the 4U beamline equipped with a Fresnel zone plate beam-focusing apparatus and a R647P photomultiplier tube detector with a P43 scintillator. The dwell time and the scanning pitch were 2 msec and 0.2 μm step, respectively.

A typical STXM image of the cross-section thin film of the vulcanized natural rubber sheet at 285.2 eV is shown in Fig. 1 (a). Heterogeneous morphology with random domain network was observed. The average domain diameter was approximately 1 μm. The C1s STXM spectra exhibits a sharp absorption peak at 285.2 eV and a broad absorption at 288 eV (Fig. 1 (b)). The absorptions are attributed to C-Hπ* signals from unsaturated C-C double bonds in poly(cis-1,4-isoprene)[2]. Because the base line absorption is even, the OD contrast would be attributed to the density inhomogeneity nor the uneven thickness. The C-Hπ* signals in the domains was stronger than that of continuous matrix region. The NR particles would intrinsically involve radial density inhomogeneity. Meanwhile, the protein and lipids in the original NR latex particles accumulate at the particle boundary leading to the reduction of poly(cis-1,4-isoprene) density in the boundary. The NR particles coalesce in the NR sheet production process to produce the low density continuous network, however, the particle cores would remain without fusion to yield the high density domain regions.

As shown in the above results, we successfully unraveled the density heterogeneity in the NR bulk by means of STXM imaging.

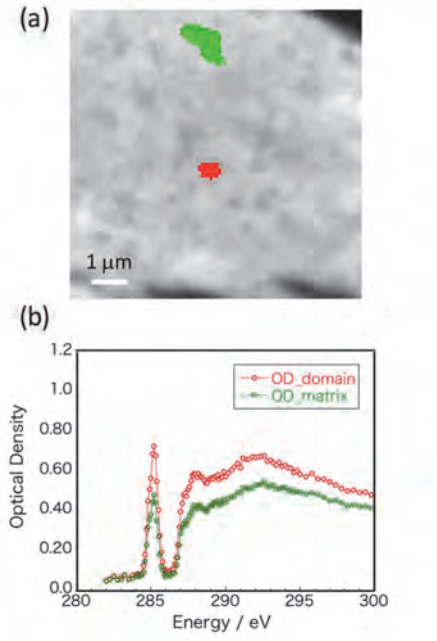

Fig. 1. Cross section of natural rubber sheet. (a) STXM micrograph (10 x 10 mm) at 285.2 eV. (b) C1s absorption spectra of the dark domains (red) and bright matrix (green) regions.

[1] S. Kumarn, N. Churinthorn, A. Nimpaiboon, M. Sriring, C. C. Ho, A. Takahara and J. Sakdapipanich, Langmuir **34** (2018) 12730.

[2] S. G. Urquhart, A. P. Hitchcock, A. P. Smith, H. W. Ade, W. Lidy, E. G. Rightor and G. E. Mitchell, J. Electron Spectros. Relat. Phenom. **100** (1999) 119.

BL4B

Multi-electron–Ion Coincidence Spectroscopy Applied to Metastability of Carbonyl Sulfide Dications

Y. Hikosaka[1] and E. Shigemasa[2]

[1] *Institute of Liberal Arts and Sciences, University of Toyama, Toyama 930-0194, Japan*

[2] *Institute for Molecular Science, Okazaki 444-8585 Japan*

Carbonyl sulfide is one of the molecules whose dications are known to be stable in the μs regime. A theoretical calculation predicted that many OCS^{2+} electronic states have potential energy surfaces with local minima [1]. In practice, high-resolution Auger spectroscopy [2] and photoelectron-photoelectron coincidence spectroscopy [1,3] have revealed the vibrational structures of several electronic states in OCS^{2+}. Kaneyasu et al. have already investigated the metastability and fragmentation of the OCS^{2+} states by Auger electron-ion coincidence spectroscopy [4]. However, overlapping Auger structures from the different S2p core-hole states, as well as the moderate energy resolution, obscures the metastability of individual electronic states. In this study, we applied multi-electron-ion coincidence spectroscopy to the S2p Auger decay in OCS and revealed the metastability of each electronic state [5].

The two-dimensional map in Fig. 1 shows correlations between the OCS^{2+} dication states and times-of-flight of ions, derived from the triple coincidences among S2p photoelectron, Auger electron, and ion. On this map, coincidence with OCS^{2+} ion is remarkably seen for the low-lying dication states around a binding energy of 32 eV. On the other hand, formations of fragment ions are remarkable above a binding energy of 35 eV. These observations basically confirm the findings by Auger electron-ion coincidence spectroscopy [4].

The band around a binding energy of 32 eV consist of three dication states ($X^3\Sigma^-$, $a^1\Delta$ and $b^1\Sigma^+$) resulting from the removals of two electrons from the 3π orbitals. A closer inspection on the coincidence yields reveals that only the highest-lying $b^1\Sigma^+$ state dissociates into fragments in the μs regime, though the fraction of the dissociation path is very weak. The calculated potential energy surfaces of these three states have all deep wells, and efficient tunneling dissociation only for the $b^1\Sigma^+$ state is not likely. The potential energy curve of the $b^1\Sigma^+$ state along CS stretch intersects that of the $1^1\Pi$ state [1]. The dissociation of the $b^1\Sigma^+$ state in the μs regime possibly results from the conversion into the $1^1\Pi$ state. Since the crossing point of the two potential energy curves locates around 2 eV above the potential minima of the $b^1\Sigma^+$ state [1], the heterogeneous predissociation should be extremely inefficient and thus proceeds in the μs regime.

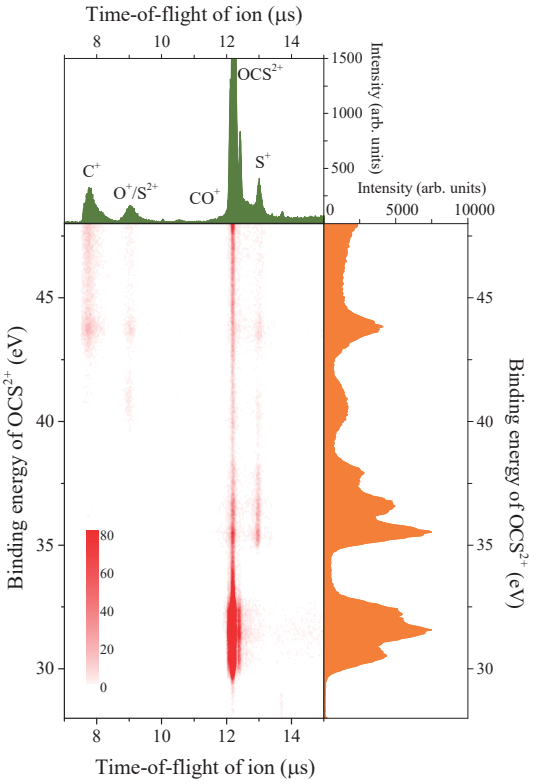

Fig. 1. Two dimensional map showing correlations between the OCS dication states (right panel) and time-of-flights of ions (top panel), derived from the triple coincidences among S2p photoelectron, Auger electron, and ion.

[1] V. Brites, J. H. D. Eland and M. Hochlaf, Chem. Phys. **346** (2008) 23.
[2] V. Sekushin, R. Püttner, R. F. Fink, M. Martins, Y. H. Jiang, H. Aksela, S. Aksela and G. Kaindl, J. Chem. Phys. **137** (2012) 044310.
[3] J. H. D. Eland, Chem. Phys. **294** (2003) 171.
[4] T. Kaneyasu, M. Ito, Y. Hikosaka and E. Shigemasa, J. Korean Phys. Soc. **54** (2009) 371.
[5] Y. Hikosaka and E. Shiegemasa, Int. J. Mass Spectrom. **439** (2019) 13.

BL4B

Pulsed Electron Extraction Introduced into a Magnetic Bottle Time-of-flight Electron Spectrometer

Y. Hikosaka
Institute of Liberal Arts and Sciences, University of Toyama, Toyama 930-0194, Japan

Multi-electron coincidence spectroscopy using a magnetic bottle time-of-flight electron spectrometer [1] is one of the most powerful means to study the multi-electron emission processes of atoms and molecules. The magnetic bottle electron spectrometer captures electrons over 4π-sr. solid angle by utilizing the magnetic mirror effect, and the electron energy analysis is based on electron time-of-flight measurement. A pulsed light source is thus required for the use of a magnetic bottle spectrometer. The single-bunch operations of synchrotron storage rings provide light pulses applicable to the electron time-of-flight measurement. However, the circumference of the used storage ring limits the periodicity of the light pulses (178 ns for the UVSOR-III ring), and the periodicity is usually shorter than the times-of-flight of slow electrons measured with a magnetic bottle electron spectrometer of a-few-meter length. For example, the single bunch operation of the UVSOR-III ring provide light pulses with periodicities of 178 ns, while a slow electron (<1 eV) takes several μs for a-few-meter flight.

In this work, a novel method to measure long electron time-of-flight with short-cycle light pulses is established [2]. In the method, a virtual stretch of light pulse intervals is achieved by pulsed extraction of electrons. Here, the observations of electrons are mostly precluded by a DC retardation electric field and are periodically allowed by applying negative voltage pulses to drop the potential at the electron source region.

The performance of the pulsed extraction method was evaluated by measuring electrons emitted from the Xe $4d_{5/2}^{-1}6p$ resonance at a photon energy of 65.110 eV. Figure 1 shows the time-of-flight spectrum of all the electrons measured with the pulsed extraction method, compared with that by the conventional way (no extraction pulse and no retardation voltage). On the measurement by the pulsed extraction, the negative voltage pulses of -70 eV were applied to the electrodes, under a DC retardation voltage of -70.0 V. The spectrum obtained by the conventional way exhibits cyclic structures resulting from the 178-ns repetition of light pulses. Severe overlaps of slow electrons construct the large background structure lying below the sharp peaks. In contrast, the overlaps are effectively removed in the spectrum measured with the pulsed extraction method, where the absolute times-of-flight of the electrons are determined. Sharp peaks in 300-450 ns result mainly from the spectator Auger decays of Xe $4d_{5/2}^{-1}6p$ into Xe^+ $5p^{-2}6p$, and the broad structure centered at around 500 ns contains slower electrons emitted on the formation of high-lying Xe^+ states and on their subsequent decay. Weak cyclic peaks, which are noticeable in the region of >800 ns, are due to the valence photoionization by the second-order light. The emitted 5p photoelectrons have a larger kinetic energy than the retardation voltage, and thus the detections cannot be precluded.

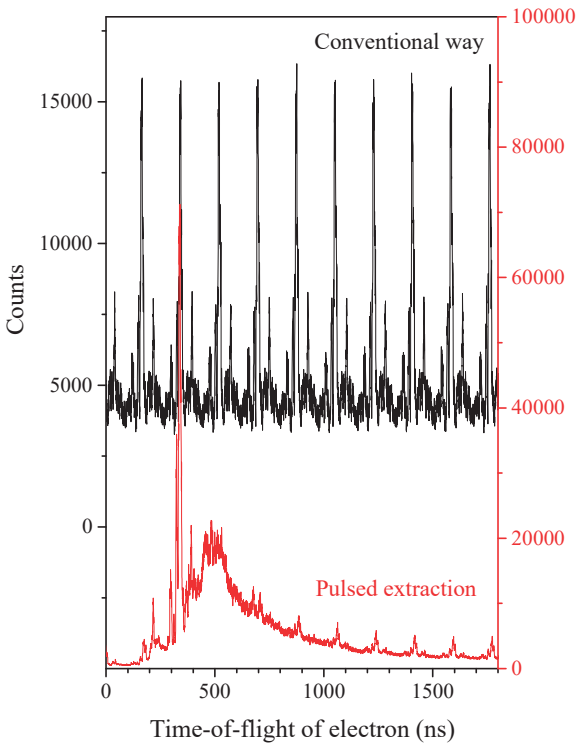

Fig. 1. Time-of-flight spectra of all electrons emitted from Xe at the photon energy for the $4d_{5/2}^{-1}6p$ resonance (65.110 eV), with the conventional way (in black) and the pulsed extraction method (in red).

[1] J. H. D. Eland, O. Vieuxmaire, T. Kinugawa, P. Lablanquie, R. I. Hall and F. Penent, Phys. Rev. Lett. **90** (2003) 053003.
[2] Y. Hikosaka, in preparation.

BL4B

Double Auger Decay from the Xe $4d_{5/2}^{-1}6p$ Resonance Studied by Multielectron Coincidence Spectroscopy

Y. Hikosaka
Institute of Liberal Arts and Sciences, University of Toyama, Toyama 930-0194, Japan

Auger decay is the main decay pathway from inner-shell excited states in light atoms, where two Auger electrons are ejected with a sizable probability. Multi-electron coincidence spectroscopy using a magnetic bottle time-of-flight electron spectrometer is a powerful means to investigate the double Auger decay mechanism. In this work, the double Auger decay of the Xe $4d_{5/2}^{-1}6p$ resonance is studied with multielectron coincidence spectroscopy [1].

Figure 1 shows the coincidences of the two Auger electrons emitted in the resonant double Auger decay. In the two-dimensional map, the formation of individual Xe^{2+} states by the direct path in the resonant double Auger decay appear as diagonal stripes. This is because the two Auger electrons simultaneously emitted share continuously the available energy which corresponds to the energy difference between the initial Xe $4d_{5/2}^{-1}6p$ state and a final Xe^{2+} state. The locations of the diagonal stripes for the formations of the Xe^{2+} $5p^{-2}$ and $5s^{-1}5p^{-1}$ states are indicated on the two-dimensional map. Intense spots are exhibited on these diagonal stripes. The cascade path in the resonant double Auger decay produces these spots, where the coordinates of the spots are defined by the discrete kinetic energies of the two Auger electrons. For most spots, the fast electrons are emitted in the first-step decay into Xe^{+} states lying above the Xe^{2+} threshold, and the slow electrons are ejected in the subsequent decay of the Xe^{+} states into low-lying Xe^{2+} states.

The projection of the coincidence counts in the two-dimensional map onto the horizontal axis is potted in the top panel of Fig. 1. The projection spectrum delineates the structure of the Xe^{+} states formed intermediately in the cascade path. These Xe^{+} structures have been revealed by conventional Auger spectroscopy in some more detail [2]. The sharp peaks lying around 13 eV and 24 eV are assigned to $5s^{-2}(^1S)6p$ and $5s^{-1}5p^{-1}(^1P)6p$, respectively, where the excited electron behaved as a spectator on the Auger electron emission. The structure around 20 eV consists of many Xe^{+} states whose dominant configuration is $5p^{-3}5d6p$. While conventional Auger spectroscopy locates also the second-step Auger transitions from these intermediate Xe^{+} states into final Xe^{2+} states [2], more unambiguous identifications of the cascade pathways can be made from the features on the two-dimensional map. The decays from $5s^{-1}5p^{-1}(^1P)6p$ and $5s^{-3}5d6p$ into Xe^{2+} $5p^{-2}$ states are exhibited as intense spots lying on the diagonal stripes for the final Xe^{2+} formations. The intensities of the spots imply that the $5s^{-1}5p^{-1}(^1P)6p$ state decays with a similar intensity into the $^3P_2$, $^3P_{0,1}$ and $^1D_2$ final states, but much weakly into the $^1S_0$ state. The preference in the decay channels differs among different $5p^{-3}5d6p$ states.

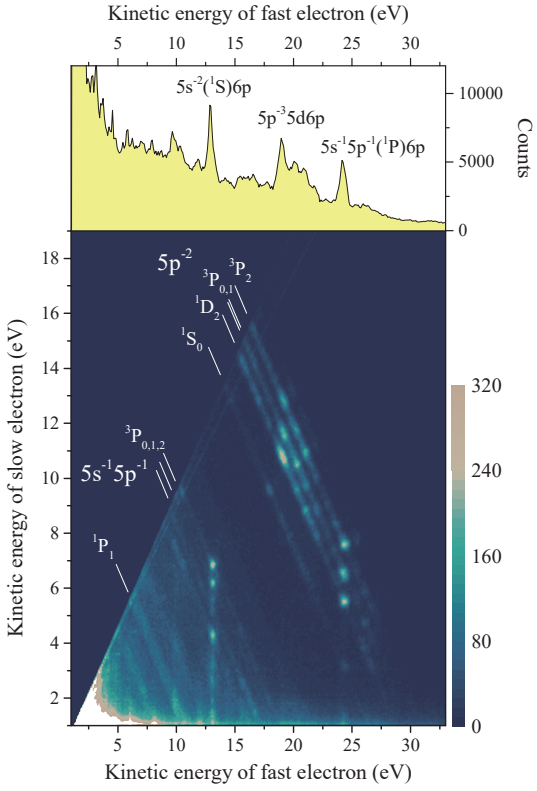

Fig. 1. Energy correlation map between two Auger electrons emitted in the resonant Auger decay from the $4d_{5/2}^{-1}6p$ resonance in Xe. The projection of the coincidence counts in the two-dimensional map onto the horizontal axis is shown in the top panel. The structures seen in the projection spectrum depict the Xe^{+} states formed intermediately in the cascade path of the resonant double Auger decay.

[1] Y. Hikosaka, in preparation.
[2] S. Osmekhin *et al.*, J. Electron Spectrosc. Relat. Phenom. **161** (2007) 105, and references therein.

BL4B

Critical Absorbed Dose of Resinous Adhesive Material Towards Non-Destructive Chemical-State Analysis Using Soft X-Rays

H. Yamane[1], M. Oura[1], N. Yamazaki[2], K. Hasegawa[3], K. Takagi[4] and T. Hatsui[1]
[1]*RIKEN SPring-8 Center, Sayo 679-5148, Japan*
[2]*Research & Innovation Center, Mitsubishi Heavy Industries, Ltd., Yokohama 220-8401, Japan*
[3]*Research & Innovation Center, Mitsubishi Heavy Industries, Ltd., Nagoya 455-8515, Japan*
[4]*Fixed Wing Aircraft Engineering Department, Mitsubishi Heavy Industries, Ltd., Toyoyama 480-0202, Japan*

Epoxy resins are the most common matrix materials for high-performance composites and adhesives. Tetraglycidyl-4,4'-diaminodiphenylmethane cured by 4,4'-diaminodiphenylsulfone (TGDDM-DDS) is an archetypal model material for the adhesive bonding. Because the oxygen element plays a crucial role in the chemical interaction and the resultant bonding strength at adhesive interfaces, the O K-edge X-ray absorption spectroscopy (XAS) is one of reliable techniques to understand the chemical interaction at adhesive interfaces. In this work, we performed the quantitative examination of the radiation damage on TGDDM-DDS for the precise analysis of the local chemical state using soft X-rays.

The total-electron-yield (TEY) XAS experiment was performed at BL4B. In the present work, the resolving power ($h\nu/\Delta E$) at $h\nu$ = 500 eV, the photon flux (N_{ph}), and the photon spot size at the surface (S) were 2500, 6×10^9 ph/s and 0.847 mm^2, respectively. The TGDDM-DDS was obtained by the curing reaction after stirring the uncured TGDDM with the DDS curing agent. To avoid the charging effect in TEY-XAS, we made the conductive path between the sample surface and the ground by pasting the Al- covered carbon tape nearby the measurement spot.

Figure 1 shows the O K-edge TEY-XAS spectra for TGDDM-DDS at 300 K as a function of the X-ray dose time (t_{dose}). The XAS pre-edge structure at $h\nu$ = 532.6 eV was not observable for the uncured TGDDM and DDS, and was found to originate from the curing process of TGDDM-DDS, that is, formation of the OH group and the possible oxidation, as confirmed by the fluorescence-yield XAS. The TEY-XAS spectra show the evidence for the radiation damage; the pre-edge structure at $h\nu$ = 532.6 eV gets weakened with t_{dose}. The XAS intensity plot at $h\nu$ = 532.6 eV as a function of t_{dose} exhibits the exponential decay, as shown in the inset of Fig. 1. Here, the XAS intensity (I_{XAS}) plot can be fitted by

$$I_{XAS} = I_{inf} + C\exp(-t_{dose}/t^c_{dose}) \qquad (1),$$

where I_{inf}, C, and t^c_{dose} are the XAS intensity at the saturated damage region, a constant, and the critical dose time for the chemical change, respectively [1]. The least-squares fitting using Eq. (1) with I_{XAS} = 1.0 at t_{dose} = 0 s gives I_{inf} = 0.853, C = 0.147, and t^c_{dose} = 4968 s. The critical flux density ($N_{ph}\,t^c_{dose}/S$) is thus determined as 3.68×10^{13} ph/mm^2.

The kinetic energy released in materials (kerma, K) is expressed as the product between the accumulated photon flux and the absorbed energy by one photon,

$$K = N_{ph}\,t_{dose} \times h\nu\,(1-T)/(\lambda\,S\,\rho) \qquad (2),$$

where T, λ, and ρ are the transmission probability, the probing depth, and the material density (1.05 g/cm^3 for TGDDM-DDS), respectively. If the photoelectron attenuation length in materials (typically, nm order) is short enough with respect to the photon irradiation area, the charged-particle equilibrium would exist, and the kerma is equal to the absorbed dose (D_a), D_a/K = 1. When λ is 2~10 nm for O K-edge TEY-XAS of polymers, the transmission probability is calculated to be T = 0.99265 (λ = 6 nm) by using Ref. [2]. These parameters give the critical absorbed dose (D^c_a) of 3.83±0.01 MGy. The small error in D^c_a of ±0.01 (less than 0.3 % for D^c_a) indicates that the critical absorbed dose does not depend on the probing depth so much, if the probing depth is sufficiently shallower than the penetration depth of photons.

By using the X-ray emission spectroscopy with the highly-brilliant and well-focused soft X-ray beam at SPring-8 BL17SU (N_{ph} = 3×10^{11} ph/s, S = 0.001 mm^2), we found that the half of D^c_a is applicable for the non-destructive chemical-state analysis of adhesive materials [3]. These results indicate that the charged-particle equilibrium exists for soft X-rays in the range of at least 0.001~0.847 mm^2 beam spot.

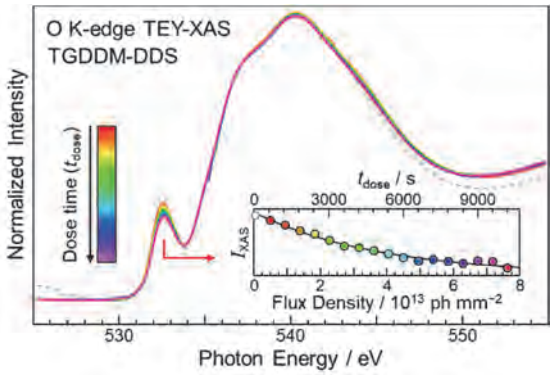

Fig. 1. O K-edge TEY-XAS spectra measured for TGDDM-DDS as a function of the X-ray dose.

[1] X. Zhang *et al.*, J. Vac. Sci. Tech. B **13** (1995) 1477.
[2] http://henke.lbl.gov/optical_constants/
[3] H. Yamane *et al.*, J. Electron Spectrosc. Relat. Phenom. **232** (2019) 11.

BL6B

Redistribution of Molecular Orbital Levels in Platinum-dithiolene Complex

T. Yamamoto[1,2,3], D. Hiraga[4], I. Arashi[1], T. Naito[1,2], T. Teshima[5], K. Tanaka[5] and R. Kato[3]

[1]*Graduate School of Science and Technology, Ehime University, Matsuyama, 790-8577, Japan.*
[2]*Geodynamics Research Center, Advanced Research Unit for High-Pressure, and Research Unit for Superconductivity, Ehime University, Matsuyama, 790-8577, Japan*
[3]*RIKEN, Wako, 351-0198, Japan*
[4]*Department of Science, Ehime University, Matsuyama, 790-8577, Japan*
[5]*UVSOR Synchrotron Facility, Institute for Molecular Science, Okazaki 444-8585, Japan*

Orbital degrees of freedom in inorganic and multi-functional solids have been attracted attention. In the field of molecular solids, on the other hand, only a few efforts have been devoted to studying the physical properties originating from the orbital degrees of freedom. We have focused on the molecular orbital (MO) of $X[Pt(dmit)_2]_2$ (dmit = 1,3-dithiole-2-thione-4,5-dithiolate and X = monovalent cation). The suppression of the charge disproportionation by the irradiation of near-infrared lights as well as the electric transitions in the infrared and near-infrared regions suggests the proximity of MO levels near Fermi energy [1].

Accumulation of our recent study concerning $X[Pd(dmit)_2]_2$ revealed that the C=C stretching modes are useful to studying how electrons occupy orbitals. We have examined the proximity and/or degeneration in the MO levels of $X[Pt(dmit)_2]_2$ based on the behavior of the C=C stretching modes. The Raman and IR spectra were observed in Instrumental Center and UVSOR, respectively. Firstly, the polarization dependence of the reflectance spectra in a single crystal was observed by using of the infrared microscope. Secondary, we observed the transmission spectra by using of the KBr pellet method. We confirmed that there is no remarkable difference between the C=C stretching modes in the reflectance spectra and those in the transmission spectra. In the last step, we observed the temperature dependence of the transmission spectra.

Figure 1 shows the transmission spectra of X = Me_4Sb (left) and Me_4P (right). The phase transition temperature of X = Me_4Sb (180 K) turned out to be lower than that of X = Me_4P (200-220 K). Factor group analysis in the low-temperature phase reveals that the charge-rich dimer ($[Pt(dmit)_2]_2^{-1-\Delta}$) and the charge-poor dimer ($[Pt(dmit)_2]_2^{-1+\Delta}$) are alternately arranged in the two-dimensional layer, which indicates no remarkable valence bond ordering in the inter-dimer interaction. This result is in contrast to the charge distributions of $X[Pd(dmit)_2]_2$, where the anti-bonding orbitals of two charge-rich dimers form valence bond. The absence of the inter-dimer valence bond in the low-temperature phase of $X[Pt(dmit)_2]_2$ indicates that the redistribution in the MO levels occurs at the phase transition temperature. Furthermore, the mutual exclusion rule cannot be applied to both IR and Raman spectra, which reveal that dimers become asymmetric originating from the disproportionation between two ligands in a monomer. This result is striking because the disproportionation of monomers might explain the conducting properties of the single component metals and superconductors.

[1] T. Ishikawa *et al*., Science. **350** (2015) 1501.
[2] T. Yamamoto *et al*., Sci. Rep. **7** (2017) 12930.

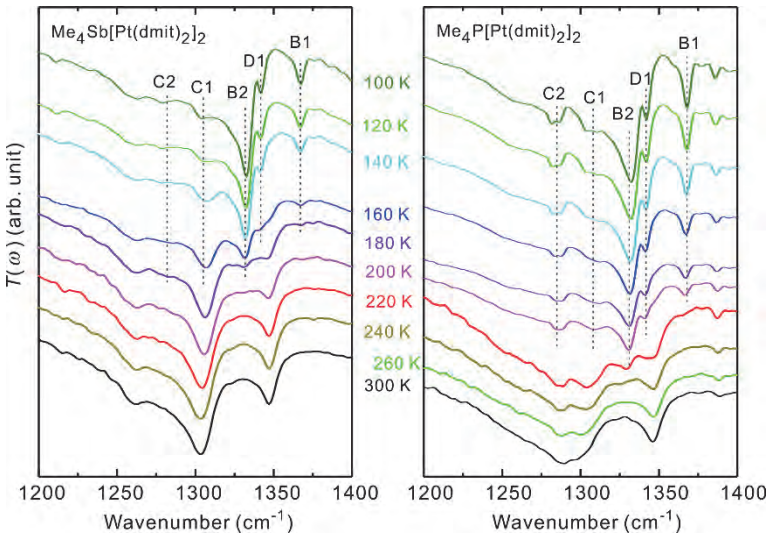

Fig. 1. Transmission spectra of X = Me_4Sb (left) and Me_4P (right).

UVSOR User 4

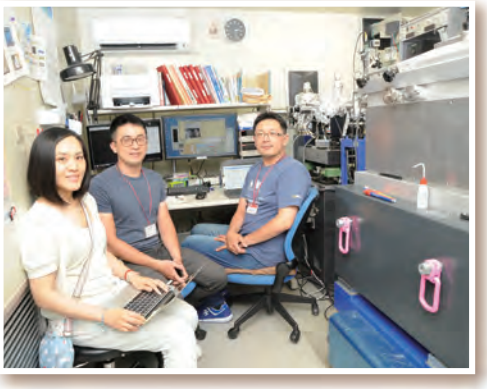

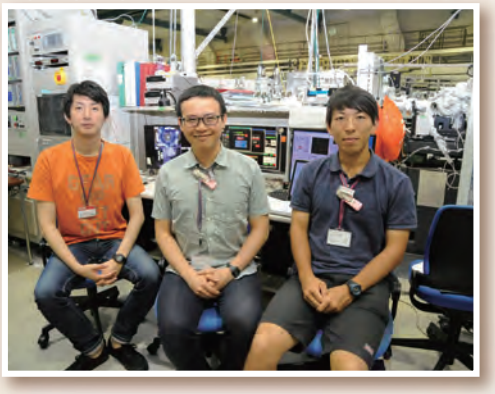

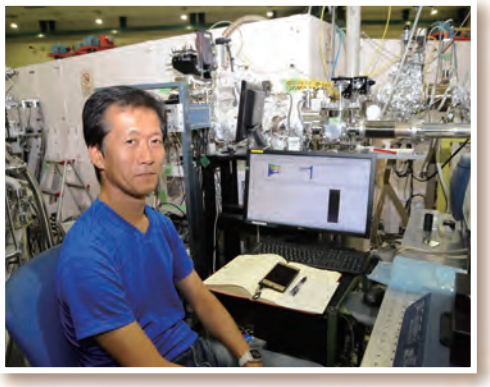

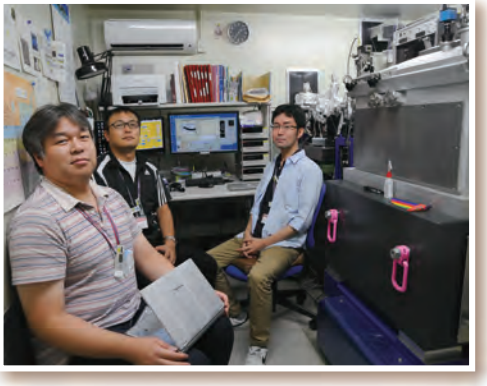

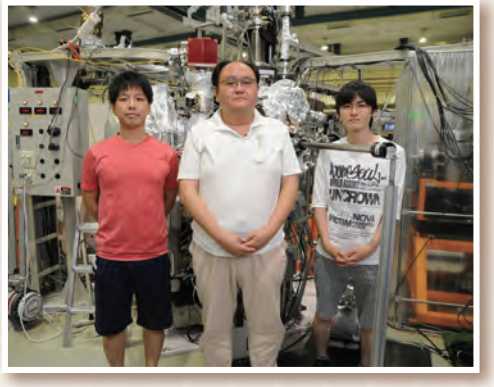

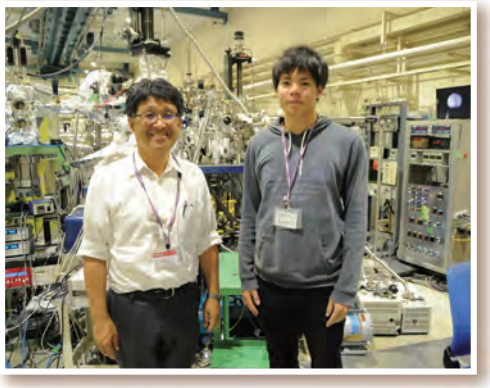

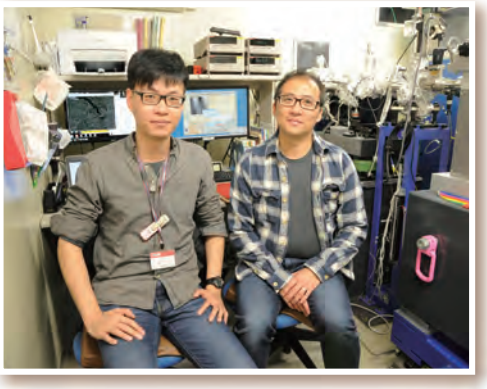

UVSOR User 5